Influence of defects on the irreversible phase transition in Fe–Pd ferromagnetic shape memory alloys

J.I. Pérez-Landazábal,[a,b,*] O.A. Lambri,[c] F.G. Bonifacich,[c] V. Sánchez-Alarcos,[a] V. Recarte[a,b] and F. Tarditti[c]

[a]Departamento de Física, Universidad Pública de Navarra, Campus de Arrosadía, 31006 Pamplona, Spain
[b]Institute for Advanced Materials (INAMAT), Universidad Pública de Navarra, Campus de Arrosadía, 31006 Pamplona, Spain
[c]Laboratorio de Materiales, Escuela de Ingeniería Eléctrica, Centro de Tecnología e Investigación Eléctrica, Facultad de Ciencias Exactas, Ingeniería y Agrimensura, Universidad Nacional de Rosario – CONICET, Avda. Pellegrini 250, (2000) Rosario, Argentina

Abstract—In Fe–Pd ferromagnetic shape memory alloys a face-centered tetragonal (fct) martensite can be obtained when cooling the face-centered cubic austenite through the martensite transition. Nevertheless, further irreversible transformation on cooling into a body-centered tetragonal (bct) martensite needs to be prevented in order to retain the shape memory properties. Differential scanning calorimetry experiments demonstrate that high temperature thermal treatments stabilize the fct phase, reducing the fct–bct transformation temperature. A large misfit between the cell parameters of fct and bct phases was determined by neutron diffraction, pointing to the critical role of dislocations in the accommodation of both phases. The presence of dislocations and its dynamics was analyzed by mechanical spectroscopy, and a relaxation peak at ∼443 K related to the dislocation movement was identified. The driving force of the relaxation process can be proposed as a dislocation dragging mechanism controlled by the migration of vacancies without break-away. Defects such as dislocations and vacancies have been shown to play an important role in changing the irreversible phase transformation temperature. A reduction in the dislocation density reduces the irreversible transformation temperature and so increases the stability range of the alloy.
© 2014 Acta Materialia Inc. Published by Elsevier Ltd. All rights reserved.

Keywords: Fe–Pd; Ferromagnetic shape memory alloys; Martensitic transformation; Dislocation dynamics

1. Introduction

Ferromagnetic shape memory alloys (FSMAs) have attracted much scientific and technological interest owing to a broad range of possible engineering applications and highly stimulating fundamental physics related to the coupling between structural, mechanical, magnetic and thermodynamic properties [1,2]. Although the Ni$_2$MnGa Heusler alloys have received most attention [3], alternative materials systems with complementary properties have also become attractive due to their higher ductility, better corrosion resistance or biocompatibility [4,5]. Concerning the Fe–Pd system, the face-centered tetragonal (fct) martensitic phase allows the magnetic shape memory effect by the reorientation of martensite variants via twin boundary motion. The fct martensite can be obtained when cooling

face-centered cubic (fcc) austenite through the martensite transition (MT) [6,7]. From the crystallographic point of view the fct martensite is indeed a bct structure; nevertheless, it is usual in the literature of FePd alloys to talk about fct when the Bain distortion of the initial fcc austenite is small. This structural transformation from fcc to fct takes place only in a very narrow compositional range (29 < at.% Pd < 32) and the transformation temperatures lie typically below room temperature (RT) [8,9]. Nevertheless, further irreversible transformation on cooling into body-centered tetragonal (bct) and cubic (bcc) martensites needs to be prevented in order to retain the shape memory properties [10–20]. Once the irreversible bct is formed, the alloy must be annealed at temperatures above 1173 K and then quenched again in order to restore the martensitic transformation. The stability range of the thermoelastic martensite is therefore restricted to temperatures between the fcc–fct and fct–bct transformation zone. Both the fcc–fct and fct–bct transformation temperatures strongly depend on composition, and just a slight increase in the Pd content may cause an abrupt decrease of both transfor-

---

* Corresponding author at: Departamento de Física, Universidad Pública de Navarra, Campus de Arrosadía, 31006 Pamplona, Spain. Tel.: +34 948168448; e-mail: ipzlanda@unavarra.es

mation temperatures [8,9]. The addition of a new element has been shown to be an effective way to control the MT temperatures of these alloys [21–28]. Nevertheless, there exist other different parameters such as internal stresses, point defects, dislocations and other bi-tri-dimensional microstructural defects that could play an important role in the characteristics of the different phase transformations and in its stability [29–36]. Epitaxial films show a tunable dependence on the strain that modifies the magnetic properties of the Fe–Pd alloys [37]. On the other hand, the motion of magnetic domains also depends on their interaction with structural defects [38]. It is the aim of the present investigation to address the impact of the intrinsic defects (in particular dislocations) on the stability of the fct martensite concerning their transition to the irreversible low temperature bct martensite.

2. Experimental

Polycrystalline ingots of nominal composition $Fe_{70}Pd_{30}$(at.%) were prepared from high purity elements by arc-melting under protective Ar atmosphere. The ingots were homogenized in vacuum quartz ampoules at 1273 K for 24 h. In order to retain the disordered γ(Fe, Pd) cubic structure, in which the MT occurs, the ingots were subjected to a 30 min annealing treatment at 1173 K in a vertical furnace, followed by quenching into iced water (AQ). Once treated, the composition of the elaborated alloys was analyzed by energy dispersive X-ray spectroscopy in a JEOL JSM-5610LV scanning electron microscope (SEM). Small samples for calorimetric measurements were obtained from disks previously cut from the center of the ingots by a slow-speed diamond saw. In order to determine the transformation temperatures, differential scanning calorimetry (DSC) measurements were carried out at a heating/cooling rate of 10 K min^{-1} in a TA Q100 calorimeter under a nitrogen protective atmosphere. Different thermal treatment cycles involving heating and cooling runs with different minimum and maximum temperatures within an interval of ~173 K and 623 K were performed. Neutron diffraction measurements were performed at the D1B installation at the Institute Laue-Langevin, Grenoble. The diffraction measurements were carried out from room temperature (RT) down to 10 K and again up to RT at a cooling/heating rate of 1 K min^{-1}. The neutron wavelength was 1.28 Å. The Fullprof program [39,40] was used for performing the profile matching in order to determine the spatial groups and the cell parameters.

Mechanical spectroscopy (MS), referred to as the internal friction method in the early literature, involves the simultaneous measurement of damping, Q^{-1} (or internal friction) and natural frequency (f) as a function of temperature and/or strain [41–45]. Measurements were performed in a mechanical spectrometer based on an inverted torsion pendulum under Ar at atmospheric pressure. The maximum strain on the sample surface was 5×10^{-5}. The measurement frequency was ~4 Hz (except for measurements performed to obtain the activation energy of the relaxation processes). The heating and cooling rates employed in the tests were 1 K min^{-1}. Damping can be calculated from the slope of the natural logarithm of the decaying amplitudes vs. time, such that [41,42].

$$\ln(A_n) = \ln(A_0) - \pi Q^{-1} n \tag{1}$$

where A_n is the area of the nth decaying oscillation, A_0 is the initial area of the starting decaying oscillation and n is the period number. For all these measurements the same initial and final values of the decaying amplitudes were used to avoid distortions linked to the appearance of amplitude-dependent damping (ADD) effects [45]. ADD, i.e. damping as a function of the maximum strain on the sample, ε_0, was calculated from Eq. (2) [45–47]:

$$Q^{-1}(\varepsilon_0) = -\frac{1}{\pi} \frac{d(\ln(A_n))}{dn} \tag{2}$$

The decaying of the oscillations was performed at constant temperature ($T \pm 0.5$ K). Polynomials were fitted to the curve of the decaying areas of the torsional vibrations as a function of the period number by means of chi-square fitting. Subsequently, Eq. (2) was applied. Polynomials of degree higher than 1 indicate that Q^{-1} is a function of ε_0, leading to the appearance of ADD effects, as can be inferred easily. This procedure allows us to obtain damping as a function of the maximum strain (ε_0) from free decaying oscillations [45–47]. The strength of the ADD behavior can be determined through the average slope of the $Q^{-1}(\varepsilon_0)$ curve using the S coefficient [45–47]:

$$S = \frac{\Delta Q^{-1}}{\Delta \varepsilon_0} \tag{3}$$

where ΔQ^{-1} is the damping change corresponding to the full amplitude changes $\Delta \varepsilon_0$ measured in the whole oscillating strain range. Depending both on the oscillating strain level (usually higher than 10^{-6}) and on the measuring temperature, the damping can be either amplitude-independent or amplitude-dependent. ADD is usually a consequence of interaction processes involving mobile dislocations through thermally activated mechanisms. The thermally assisted break-away of dislocations from weak pinning points is one such example. Mechanisms involving the dragging of jogs by screw dislocations, or the pinning by large precipitates or other blocked dislocations, lead to nearly amplitude-independent damping processes [48,49].

The elastic shear modulus, G, was calculated from the proportionality relationship with the square of the natural oscillating frequency (f). This relation for the case of a bar of rectangular section is [45,50,51]:

$$G = \frac{(2\pi)^2 f^2 l\, II}{ka^3 b} \alpha f^2 \tag{4}$$

where k is a constant which depends on the ratio b/a, II is the moment of inertia of the oscillating system, l is the length of the sample and a and b are the half thickness and width of the sample, respectively.

3. Results and discussion

The structural transformations have been studied by DSC measurements. Fig. 1a shows DSC thermograms for the sample in the as-quenched state. The exothermic (endothermic) peak observed on cooling (heating) corresponds to a direct (reverse) thermoelastic MT. The measured enthalpy is 0.8 J g^{-1} and corresponds to the full transformation from fcc austenite to fct martensite [28]. In order to determine the stability of the fct phase, the next measurement was performed down to a lower temperature limit, as shown in Fig. 1b. As expected, the thermogram exhibits two exother-
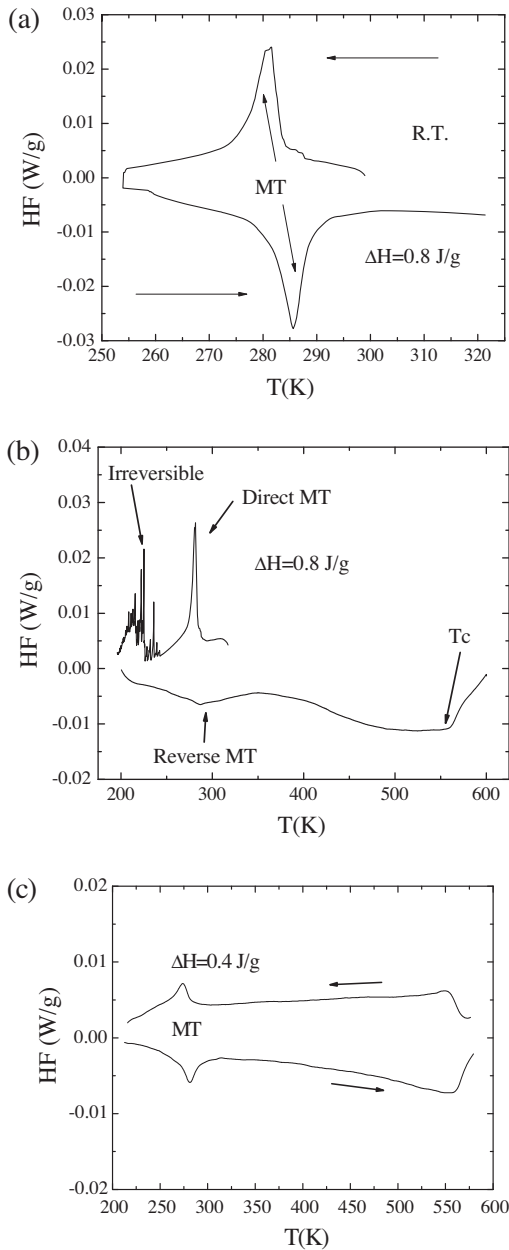
the microstructure is a mixture of bct phase and austenite or martensite fct depending on the temperature. The Curie temperature of the alloy at $T_c = 560$ K can also be identified in Fig. 1b. An intermediate thermal treatment at 603 K by heating in situ in the DSC restores partially the MT as observed in Fig. 1c, reducing the transformation temperature and the width of the transformation peak. Comparing the involved enthalpies before and after heating up to 603 K, ∼50% of the material transforms between austenite and martensite and 50% of the alloy has transformed to the irreversible bct phase. The thermal treatment could produce different microstructural changes such as atomic ordering, dislocation recovery, internal stresses reduction and so on [52,53].

In order to analyze in more detail the effect of post-quench thermal treatments on the MT, DSC thermograms on as-quenched samples subjected to several consecutives heating/cooling thermal cycles were performed. DSC thermal cycles were carried out between 253 K and a maximum temperature (T_{aging}) higher for each new cycle, see Fig. 2a. This procedure makes it possible to observe "in situ" the evolution of temperature corresponding to the maximum of the fcc–fct MT peak on cooling, T_p^C, and heating, T_p^H, as a consequence of each thermal treatment at the aging temperature (T_{aging}). Fig. 2b shows the change in T_p both on cooling and on heating as a function of the post-quench aging temperature, T_{aging}. Although the change is small, the

Fig. 1. (a) Cooling–heating DSC thermogram for a Fe–Pd sample in the as-quenched state. The lower temperature is above the starting point of the irreversible transformation. (b) Subsequent DSC thermogram measured first on cooling from RT to detect the irreversible bct phase and then on heating. (c) DSC corresponding to a sample with an intermediate thermal treatment at 603 K (heating in situ in the DSC).

mic processes on the first cooling ramp: the high temperature peak associated to the forward fcc–fct transformation and a low temperature series of peaks corresponding to the burst-like fct–bct irreversible transformation [27]. The irreversibility is confirmed by the reduction on the heating curves of the corresponding endothermic peak linked to the reverse MT to the fcc austenitic phase. On heating, the MT is broad and the estimated transformation enthalpy is $\Delta H = 0.4$ J g^{-1}, half the original one. Therefore, the high and low temperature exothermic processes must be definitively linked to the reversible and irreversible transformation, respectively. Once the irreversible phase is produced,
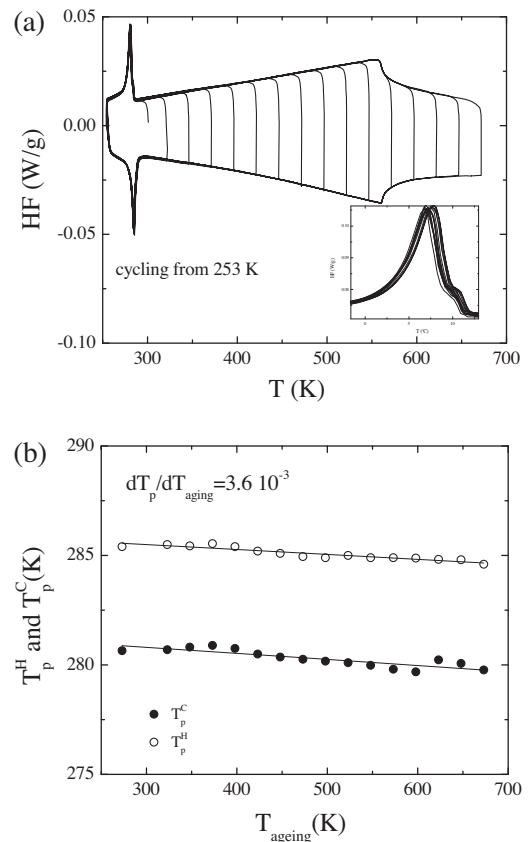

Fig. 2. (a) DSC thermograms performed on several consecutive thermal cycles on a sample in the as-quenched state increasing the maximum measuring/aging temperature (T_{aging}). The inset shows a zoom of the DSC response for the temperature range where MT develops. (b) Change in the transformation temperatures as a function of the post-quench aging temperature (T_{aging}).

transformation temperature slightly decreases with the aging temperature. It is also worth mentioning that the thermal hysteresis (see Fig. 2b) associated to the MT remains constant ($T_p^H - T_p^C \sim 5$ K) for the different aging temperatures. Finally, Fig. 3 shows the effect of a previous annealing treatment to 673 K on the irreversible phase transformation. The bct irreversible phase can barely be observed on cooling down to 193 K. Only a small quantity of "burst" peaks can be measured below 198 K (see inset in Fig. 3). On the second cooling down the "burst" peaks obviously disappear and, due to the small fraction of bct formed, the MT peaks remain nearly unaffected. So the effect of the aging treatments is to stabilize the fct phase, increasing the temperature range where the reversible MT can be produced. Indeed, this is an important point to be noted for technological applications.

The phase evolution has been also determined by neutron diffraction experiments performed on cooling from RT down to 10 K and subsequently on heating from 10 K to RT. Fig. 4 shows a three-dimensional picture (intensity, 2θ and temperature) of the phase evolution observed "in situ". On cooling the $(2\,2\,0)_{fcc}$ reflection splits on two new reflections corresponding to the fct structure. On further cooling, the intensity of these fct reflections decreases as the bct phase forms, but they do not become zero even after cooling down to 10 K. This means that not all the fct phase transforms into the bct structure. On the other hand, when the sample is heated again to RT, the reverse fct–fcc transformation occurs and then the fct reflections merge again into the reflection whereas the reflections linked to the irreversible phase indeed persist. The fraction of fct martensite transforming into the bct phase has been estimated by comparing the integrated intensity of a fcc reflection at 320 K before and after cooling down to 10 K and the 53% found agrees with the previous values determined by calorimetry. The fitting of the textured spectra using a matching profile procedure (Fullprof) allows us to determine the temperature dependence of the cell parameters. The Bain distortion describes the MT in this kind of alloy but the fct phase is obviously an inadequate crystallographic description of the martensitic phase. In fact the correct structure should be a bct structure. Nevertheless, the notation fct is used in the literature to describe the reversible martensite in contrast to the irreversible one that appears on cooling below a critical temperature. In order to see the changes of the lattice
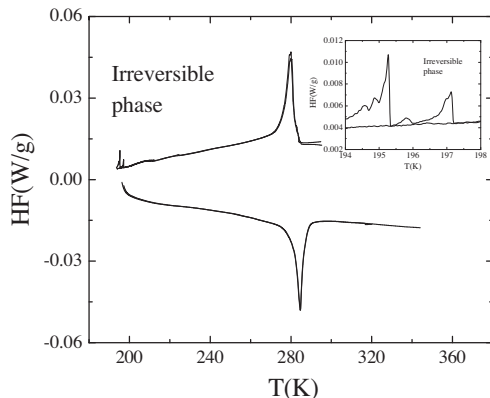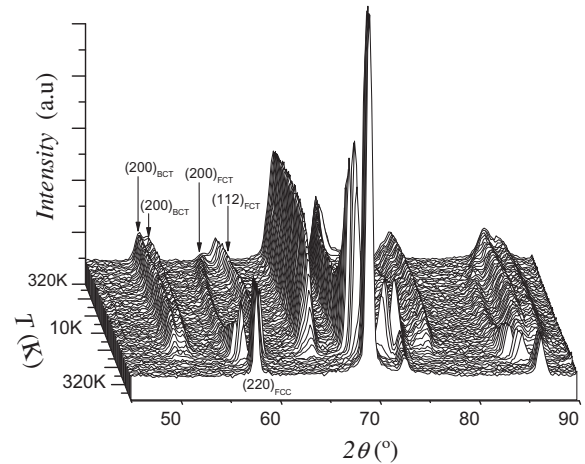

Fig. 4. Three-dimensional thermodiffractogram showing the splitting of fcc reflection at the fcc–fct transition and the appearance of the irreversible bct reflections at the fct–bct transformation temperature.
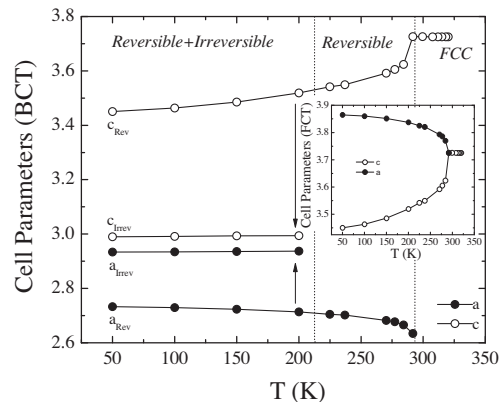

Fig. 5. Temperature dependence of the bct (P4/mmm) lattice parameters. The inset shows the parameter evolution described using the fct cell parameters.

parameter in the irreversible transition, the right bct (P4/mmm space group) description of crystallographic martensitic structures has been used. Fig. 5 shows the "a" and "c" cell parameters of the bct structure as a function of temperature. On the other side, the inset in Fig. 5 shows the parameter evolution described using the more usual fct cell parameters on the reversible-to-irreversible-transformation range. The reversible martensite is stable at ~75 K below the MT transition temperature and the "c" and "a" parameters decrease and increase, respectively, on cooling. The transition to the irreversible phase is accompanied by a sudden change of both lattice parameters, as shown in Fig. 5 by arrows. At low temperatures both the reversible and the irreversible phases coexist. The large misfit between both phases should be adjusted by the creation of dislocations or twin boundaries to relieve the otherwise enormous stresses generated in the interphase area. Indeed, it is well known that the misfit strain from the appearance of a second phase leads to a plastic relaxation zone in order to balance the transformation stress and strain energy related to the transition [31–36]. In fact, before the transition, dislocations must play an important role in order to assist the accommodation of the bct phase on further cooling. The

Fig. 3. DSC thermograms performed on a sample aged at 673 K. The inset shows a magnification of the "burst" peak low temperature range.

larger the quantity of dislocations in the alloy, the easier should be the irreversible transition to the bct phase. So it could be expected that a low density of dislocations must produce a reduction in the transition temperature. This agrees with the previous results found by calorimetry, where a thermal treatment of the alloy at 673 K reduces the defects density and reduces the transition temperature to the irreversible phase.

In any case, this kind of analysis requires a more systematic study of the dislocation behavior and its influence on the transformation. Consequently, mechanical spectroscopy, which is a powerful and sensitive technique to analyze the dynamics of structural defects like dislocations, was used [41,42,48,49]. Fig. 6a shows damping spectra measured on warming from 253 K up to 603 K during two consecutive thermal cycles. During the first heating run (open circles), a peak related to martensitic transformation appears below room temperature. In addition, another damping peak at ~443 K develops, called hereafter P_1. Several works exist in the literature to analyze the origin and characteristics of the MT damping peak [49,54,55]. Nevertheless, the P_1 peak has not been studied previously. Efforts performed in this work are devoted to analyzing this second process which occurs above the MT temperature. The performed DSC experiments seem to show that the physical mechanism controlling the P_1 relaxation must influence the fcc–fct and fct–bct transitions. In the second warming run (black circles), the sample has been subjected to a thermal treatment at 603 K during the first heating, and the P_1

peak decreases its height markedly. In fact, the peak height during the first cooling down from 603 K was similar to the height measured during the second warming run (not shown here for the sake of clarity). In both heating runs the shear modulus (Fig. 6b) increases with the temperature, showing overall larger values during the second heating run. During the first heating run, the shear modulus curve shows a first stage linked to the MT at around RT, a second stage between RT and 548 K and a clear slope change above 548 K. On the second one the MT can be also observed but the slope change disappears.

Mechanical spectroscopy thermal cycles performed on a sample cooled below the irreversible transformation range, Fig. 7, shows the same behavior as that shown in Fig. 6 for a sample free of irreversible phase. In this case the sample above room temperature shows a mixture of austenite and irreversible bct martensite (see Figs. 4 and 5). Nevertheless, the presence of the irreversible phase reduces the net height of P_1 damping peak, indicating that this P_1 peak must be related to the intrinsic properties of the austenitic phase. In thermal cycles performed on a sample cooled to 173 K, Fig. 7, the maximum temperature reached in each consecutive cycle was increased in the following values: 603 K, 673 K and 773 K. The higher the temperature of the thermal treatment, the lower the damping value. This seems to indicate that the mechanism responsible for this damping process must be related to an unstable thermodynamic state [49,56]. On the other hand, the shear modulus,
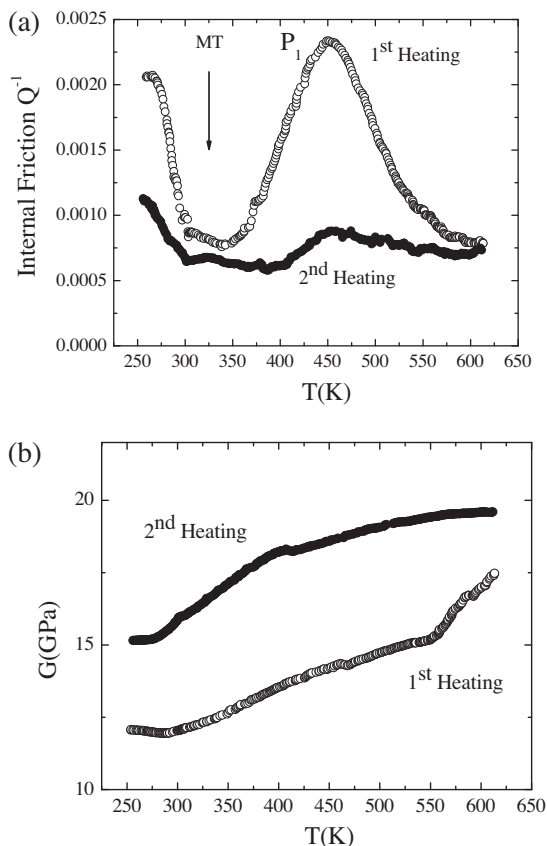

Fig. 6. Damping Q^{-1} (a) and shear modulus G (b) measured during heating from 253 K to 603 K in two consecutives ramps for an as-quenched sample.
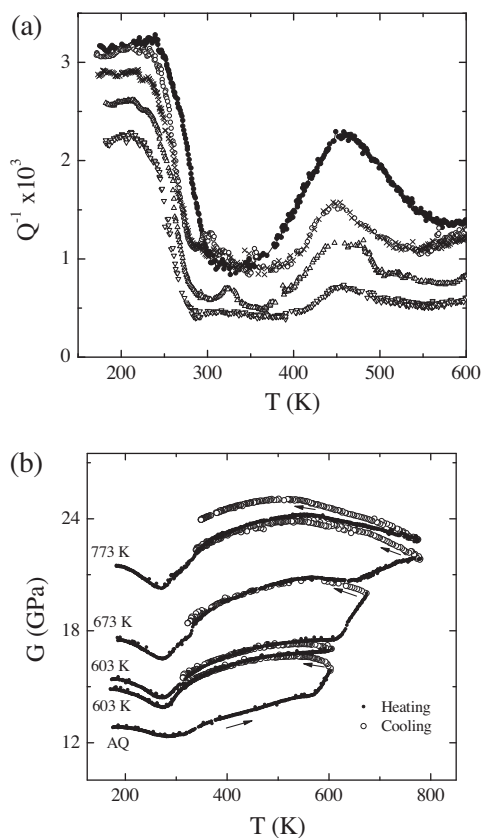

Fig. 7. Damping Q^{-1} (a) and shear modulus G (b) measured during heating from 173 K to 603 K in samples in the as-quenched state (black holes) and after heating the sample to 603 K (two consecutive times, white holes and crosses) to 673 K (upward triangle) and to 773 K (downward triangle).

Fig. 7b, increases with the temperature, showing overall larger values during the consecutive heating runs. Besides, the shear modulus measured during cooling from high temperature fits perfectly with the subsequent heating run. In any case, a continuous increase of the elastic modulus and a reduction in the damping behavior hint to a mechanism involving recovery of dislocations and defects or a precipitation processes [41,48,52,53,56,57]. Neither DSC measurements (see Figs. 1 and 2) nor X-ray diffraction experiments seem to indicate the presence of new phases during heating. Therefore, a recovery of defects could be controlling the damping behavior in this temperature range.

Fig. 8 shows the net damping P_1 peak after background subtraction corresponding to spectra shown in Fig. 7 (damping background subtraction was performed by means of Peak Fit V.4 soft [58] using cubic polynomials). As shown, the P_1 intensity depends on the thermal treatment and decreases as soon as the maximum reached temperature increases. Thermal treatments above 773 K do not reduce the peak intensity (results not shown here). Nevertheless, torsion plastic deformation performed "in situ" at the spectrometer leads not only to an increase in the whole background damping but also to an increase in the peak height of P_1 peak, see crosses in Fig. 8. As expected, a new quenching procedure restores the P_1 peak height to similar values to those shown in Fig. 6 for the as-quenched sample. Since deformation increases the damping values corresponding to the P_1 peak, dislocations are clearly a candidate responsible for the relaxation process [41–44,47].

The appearance of ADD has been checked through the S parameter for some measurements of the whole set shown in Fig. 7. Fig. 9 shows the S values as a function of temperature for the spectra corresponding to the as-quenched sample and after an annealing to 603 K. The result differs from zero just for temperatures where the martensitic phase occurs. Non-linear anelasticity is selectively related to the motion of linear/planar defects and therefore is an efficient tool of studying pinning-related phenomena [49,54,59]. The MT transformation has been analyzed in detail in different alloy systems by mechanical spectroscopy [59–61]. The higher values of S for the annealed sample shown in Fig. 9 indicate that the amount of quenched-in defects has decreased and then both the dislocations and variants
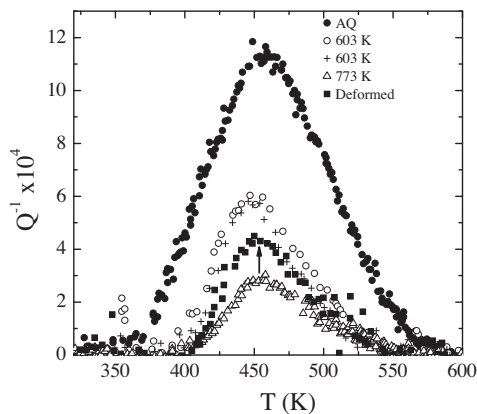

Fig. 9. ADD strength, S values, as a function of temperature.

increase their mobility. Nevertheless, within the temperature range of P_1, the S values are null, indicating that the damping occurs without amplitude-dependent effects, i.e. the damping behavior is linear. Since the mechanism responsible for the P_1 relaxation seems to involve dislocation movements, the absence of ADD effects would indicate that dislocation movement occurs without thermally activated break-away [41,42,44–48,62]. On the other hand, the behavior of the elastic modulus as a function of temperature (see Fig. 7b), where an inverse modulus dependence on temperature occurs, could indicate that the damping peak involves the dragging of point defects by the dislocation during their movement [63–65].

In order to check this point in detail, the activation energy and pre-exponential factor for the relaxation time corresponding to the P_1 peak were obtained using the peak temperature shift measured at different oscillation frequencies (see Fig. 10) [41–43]. The values measured in a sample with stabilized damping (after heating the sample to 773 K) are $E_a = (1.0 \pm 0.1)$ eV and $\tau_o = 5 \times 10^{-(13 \pm 0.5)}$ s. Indeed, above 220 K the migration and clustering of vacancies develops [66–68] and the obtained value of 1.0 eV is close to the activation energy for vacancy migration in α-Fe, ≈ 1.3 eV [66]. In addition, the calculated value of the pre-exponential factor is within the usual range for dislocation relaxation processes [41,69]. Consequently, the driving force for the development of P_1 relaxation can be proposed

Fig. 8. Internal friction Q^{-1} after background subtraction measured during heating from 173 K to 603 K in two consecutives ramps (black and white holes). A third heating to 603 K (crosses) and a subsequent heating to 773 K (triangles) are also shown. The effect of torsion plastic deformation performed in situ is shown by squares.
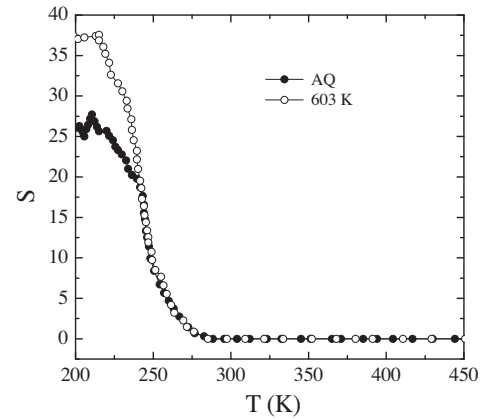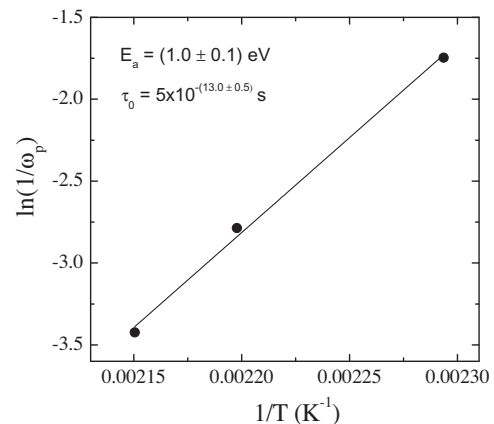

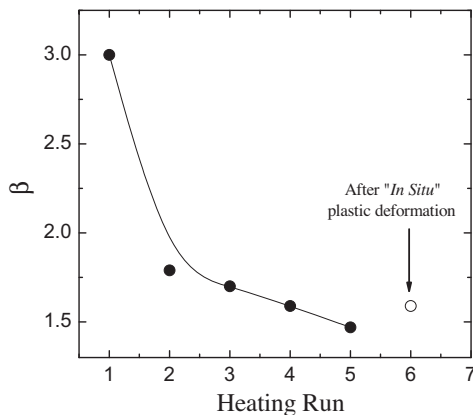**Fig. 10.** Arrhenius plot corresponding to the P_1 peak.

Fig. 11. Evolution of the $\beta = W/WD$ parameter (W is the width of the measured damping peak and WD corresponds to a single relaxation time, Debye type) as a function of the thermal treatment. Cycle 1: as-quenched sample; 2: sample heated to 603 K; 3: heated to 603 K again; 4: heated to 673 K; 5: heated to 773 K; 6: after room temperature "in situ" deformation. The full line is a visual guide.

as a dislocation dragging mechanism controlled by the migration of vacancies without break-away.

The width (β) of the P_1 peak as a function of the thermal treatment was analyzed by the ratio [41,42,47]:

$$\beta = W/WD \tag{5}$$

where W is the width of the measured net damping peak, considered to be described by a log-normal distribution function of relaxation times, and WD is the width for a Debye-type peak calculated for the previous measured activation energy. It is well known that $\beta = 1$ means that the damping peak is of Debye type, i.e. it is controlled by a single relaxation time [41–43]. The β parameter for the as-quenched sample is close to 3 and decreases markedly as the sample is annealed during the successive heating runs performed along the work, Fig. 11. The decrease in β indicates that the distribution spectra of dissipative micromechanisms are decreasing as the thermal cycles increase. This evolution is in agreement with the above exposed about the mechanism controlling P_1 peak since the thermal treatment reduces the number of dislocations and vacancies, so reducing the width of the distribution function of relaxation times. Accordingly, a plastic deformation increases again the β parameter, due to the formation of new dislocations and vacancies. Therefore, annealing of FePd samples over 600 K leads to a recovery of the structure which hinders the accommodation of the misfit strain promoted by the formation of the bct phase, giving rise to a decrease in the temperature for the appearance of the irreversible bct phase. A direct observation of the distribution and dislocation density after the different thermal treatments could help to get a deeper insight into the recovery processes and to corroborate the obtained results.

4. Summary and conclusions

The stability at low temperatures of the thermoelastic martensite in FePd alloys is restricted by the irreversible fct–bct phase transformation. DSC experiments demonstrate that a thermal treatment above 600 K clearly stabilizes the alloy, reducing the fct–bct transformation

temperature. The large misfit between the cell parameters of fct and bct phases found by neutron diffraction must be accommodated by dislocations. The presence of dislocations and their dynamics has been analyzed by mechanical spectroscopy. A relaxation peak at ~443 K related to the dislocation movement has been identified. The driving force can be proposed as a dislocation dragging mechanism controlled by the migration of vacancies without break-away. Defects such as dislocations and vacancies have been shown to play an important role in the irreversible phase transformation temperature. A reduction in the dislocation density reduces the irreversible transformation temperature and so increases the stability range of the fcc–fct reversible transformation.

Acknowledgements

References

[1] K. Ullakko, J.K. Huang, R.C. Kantner, R.C. O' Handley, V.V. Kokoring, Appl. Phys. Lett. 69 (1996) 1966.
[2] J. Ma, I. Karaman, Science 327 (2010) 1468.
[3] J. Webster, K.R.A. Ziebeck, S.L. Town, M.S. Peak, Philos. Mag. B 49 (1984) 295.
[4] R.D. James, M. Wuttig, Philos. Mag. A 77 (1998) 1273.
[5] Y. Ma, M. Zink, S.G. Mayr, Appl. Phys. Lett. 96 (2010) 213703.
[6] M. Matsui, H. Yamada, K. Adachi, J. Phys. Soc. Jpn. 48 (1980) 2161.
[7] T. Sohmura, R. Oshima, F.E. Fujita, Scr. Metall. 14 (1980) 855.
[8] M. Sugiyama, R. Oshima, F.E. Fujita, Trans. JIM 19 (1984) 585.
[9] J. Cui, T.W. Shield, R.D. James, Acta Mater. 52 (2004) 35.
[10] R. Oshima, Scr. Metall. 15 (1981) 829.
[11] R. Oshima, M. Sugiyama, J. Phys. IV 43 (1982) 383.
[12] M. Sugiyama, S. Harada, R. Oshima, Scr. Metall. 19 (1985) 315.
[13] M. Sugiyama, R. Oshima, F.E. Fujita, Trans. JIM 27 (1986) 719.
[14] S. Muto, R. Oshima, F.E. Fujita, Scr. Metall. 21 (1987) 465.
[15] R. Oshima, M. Sugiyama, F.E. Fujita, Metall. Trans. A 19A (1988) 803.
[16] S. Muto, S. Takeda, R. Oshima, F.E. Fujita, J. Appl. Phys. 27 (1988) 1387.
[17] S. Muto, R. Oshima, F.E. Fujita, Mater. Sci. Forum 56–58 (1990) 65.
[18] S. Muto, S. Takeda, R. Oshima, J. Appl. Phys. 29 (1990) 2066.
[19] K. Tanaka, R. Oshima, Mater. Trans. JIM 32 (1991) 325.
[20] R. Oshima, S. Muto, F.E. Fujita, Mater. Trans. JIM 33 (1992) 197.
[21] K. Tanaka, K. Hiraga, R. Oshima, Mater. Trans. JIM 33 (1992) 215.
[22] K. Tsuchiya, T. Nojiri, H. Ohtsuka, M. Umemoto, Mater. Trans. JIM 44 (2003) 2499.
[23] T. Wada, T. Tagawa, M. Taya, Scr. Mater. 48 (2003) 207.

[24] D. Vokoun, Y.W. Wang, T. Goryczka, C.T. Hu, Smart Mat. Struct. 14 (2005) 261.
[25] Y.C. Lin, H.T. Lee, S.U. Jen, Y.T. Chen, J. Appl. Phys. 101 (2007) 09N514.
[26] S.U. Jen, Y.T. Chen, T.L. Tsai, Y.C. Lin, J. Appl. Phys. 103 (2008) 07B902.
[27] V. Sánchez-Alarcos, V. Recarte, J.I. Pérez-Landazábal, C. Gómez-Polo, V.A. Chernenko, M.A. González, Eur. Phys. J. Special Topics 158 (2008) 107.
[28] V. Sánchez-Alarcos, V. Recarte, J.I. Pérez-Landazábal, M.A. González, J.A. Rodríguez-Velamazán, Acta Mater. 57 (2009) 4224.
[29] M.E. Gruner, P. Entel, Phys. Rev. B 83 (2011) 214415.
[30] I. Claussen, R.A. Brand, H. Hahn, S.G. Mayr, Scr. Mater. 66 (2012) 163.
[31] J.K. Lee, Y.Y. Earmme, H.I. Aaronson, K. Russell, Metall. Trans. A 11 (1980) 1837.
[32] T. Mura, Micromechanics of Defects in Solids, Martinus Nijhoff, New York, 1987.
[33] M. Shibata, K. Ono, Acta Metall. 2 (1975) 587.
[34] M. Shibata, K. Ono, Acta Metall. 25 (1977) 35.
[35] E. Patoor, D.C. Lagoudas, P.B. Entchev, L Catherine Brinson, X Gao, Mech. Mater. 38 (2006) 391.
[36] D.C. Lagoudas, P.B. Entchev, P. Popov, E. Patoor, L Catherine Brinson, X Gao, Mech. Mater. 38 (2006) 430.
[37] J. Buschbeck, I. Opahle, M. Richter, U.K. Röbler, P. Klaer, M. Kallmayer, H.J. Elmers, G. Jakob, L. Schultz, S. Fähler, Phys. Rev. Lett. 103 (2009) 216101.
[38] A. Budruk, C. Phatak, A.K. Petford-Long, M. De Graef, Acta Mater. 59 (2011) 6646.
[39] R.A. Young (Ed.), The Rietvald Method, University Press, Oxford, 1993.
[40] J. Rodriguez-Carvajal, Program FullProf. Rietveld Analysis of X rays and Neutron Powder Diffraction Patterns, Institut Laue-Langevin, 2005.
[41] R. Schaller, G. Fantozzi, G. Gremaud (Eds.), Mech. Spectrosc., Trans Tech Publications, Zurich, 2001.
[42] A.S. Nowick, B.S. Berry, Anelastic Relaxation in Crystalline Solids, Academic Press, New York, 1972.
[43] C. Zener, Elasticity and Anelasticity of Metals, University of Chicago, Chicago, IL, 1956.
[44] D.H. Niblett, J. Wilks, Adv. Phys. 33 (1960) 9.
[45] O.A. Lambri, A review on the problem of measuring nonlinear damping and the obtainment of intrinsic damping, in: J. Martinez-Mardones, D. Walgraef, C.H. Wörner (Eds.), Materials Instabilities, World Scientific Publishing, New York, 2000.
[46] B.J. Molinas, O.A. Lambri, M. Weller, J. Alloys Compd. 211–212 (1994) 181.
[47] G.I. Zelada-Lambri, O.A. Lambri, J.A. García, J. Nucl. Mater. 353 (2006) 127.
[48] J. Friedel, Dislocations, Reading, Addison-Wesley, Reading, 1967.
[49] R. De Batist, Mechanical spectroscopy, in: E. Lifshin (Ed.), Characterization of Materials, in: R.W. Cahn, P. Haasen, E.J. Kramer (Eds.), Materials Science and Technology, vol. 2B, Part II, VCH, Weinheim, 1991.
[50] C.T. Wang, Applied Elasticity, McGraw-Hill, New York, 1953.
[51] E.J. Hearn, Mechanics of Materials, Pergamon Press, Oxford, 1995.
[52] R.W. Cahn, P. Haasen, Physical Metallurgy, North-Holland, Amsterdam, 1983.
[53] D.A. Porter, K.E. Easterling, Phase Transformations in Metals and Alloys, Van Nostrand Reinhold (International), Wokingham, 1988.
[54] J. Van Humbeeck, High damping capacity due to microstructural interfaces, in: B.B. Rath, M.S. Misra (Eds.), Role of Interfaces on Materials Damping, Proc. ASM's Materials Week and TMS/AIME Fall Meeting, Toronto, 1985.
[55] J. Van Humbeeck, The martensitic transformation, in: R. Schaller, G. Fantozzi, G. Gremaud (Eds.), Mechanical Spectroscopy, Trans Tech Publications, Zurich, 2001.
[56] J. Philibert, Atoms movements, diffusion and mass transport in solids, Monographies de Physique, Les editions de Physique, Les Ulis, 1991.
[57] O.A. Lambri, J.A. García, W. Riehemann, J.A. Cano, G.I. Zelada-Lambri, F. Plazaola, Mater. Trans. JIM 52 (2011) 1016.
[58] Peak Fit, V. 4, Jandel Scientific Software, Germany, 1995.
[59] E. Cesari, S. Kustov, S. Golyandin, K. Sapozhnikov, J. Van Humbeeck, Mater. Sci. Eng. A 438–440 (2006) 369.
[60] E. Cesari, V.A. Chernenko, V.V. Kokorin, J. Pons, C. Segui, Mater. Acta Mater. 45 (1997) 438.
[61] V.A. Chernenko, C. Segui, E. Cesari, J. Pons, V.V. Kokorin, Phys. Rev. 57 (1998) 2659.
[62] A. Granato, K. Luecke, J. Appl. Phys. 30 (1959) 525.
[63] H.M. Simpson, A. Sosin, Phys. Rev. B 5 (1972) 1382.
[64] H.M. Simpson, A. Sosin, Phys. Rev. B 16 (1977) 1489.
[65] G.I. Zelada-Lambri, O.A. Lambri, P.B. Bozzano, J.A. García, C.A. Celauro, J. Nucl. Mat. 380 (2008) 111.
[66] W. Frank, A. Seeger, M. Weller, Interpretation of positron annihilation experiments on electron-irradiated α-iron in terms of self-interstitial migration in stage III. In: M.T. Robinson, F.W. Young Jr. (Eds.), Fundamentals Aspects of Radiation Damage in Metals, US ERDA CONF-751006, Oak Ridge, TN, 1976, vol. 1, p. 518.
[67] M. Weller, J. Diehl, W. Trifshäuser, Solid State Commun. 17 (1975) 1223.
[68] M. Eldrup, Application of the positron annihilation technique in studies of defects in solids, in: A.V. Chadwick, M. Terenzi (Eds.), NATO ASI Series, Plenum, New York, 1985, p. 145.
[69] G.I. Zelada, O.A. Lambri, P.B. Bozzano, J.A. García, Phys. Status Solidi A 209 (2012) 1972.